Water Science & Technology

Water Science & Technology Vol 85 No 9, 2693 doi: 10.2166/wst.2022.140

Numerical investigation of the influence of banded sand ditches on water infiltration in fine-textured soil

Yanwei Fan*, Changyan Zhang, Hujun Wei and Wen Shi

College of Energy and Power Engineering, Lanzhou University of Technology, Lanzhou 730050, China
*Corresponding author. E-mail: fanyanwei24@163.com

ABSTRACT

Enhancing rainwater infiltration is important to reduce the risk of urban waterlogging and improve the utilization rate of urban rainwater resources. Using the HYDRUS model, a mathematical model of soil water movement under a banded sand ditch pattern (the vertical excavation of a deep trench with heavy soil and filled with light soil) was created. Forty-six scenarios were designed to examine effects of sand ditch soil saturated hydraulic conductivity (K_{ss}), original homogenous fine-textured soil saturated hydraulic conductivity (K_{so}), sand ditch width (W), spacing (S), and depth (D) on the soil infiltration rate (i). Results indicate that banded sand ditches cause increased permeation and have a significant turning point 't_0' in the curve of 'i' for 't.' Taking 't_0' as the boundary, 'i' can be divided into two stages ($t \leq t_0$ and $t > t_0$), 'i' and 't,' for each stage according to the power function relationship; there is little change in power function indices, which can be fixed at 0.34 and 0.63, respectively. In addition, the coefficient has a linear relationship with K_{ss}, K_{so}, W, S, and D. Thus, an estimation model of the soil infiltration rate under a banded sand ditch pattern was proposed and verified for reliability.

Key words: banded sand ditch, HYDRUS, simplified infiltration model, water infiltration

HIGHLIGHTS

- Based on HYDRUS, a mathematical model of soil water movement under a banded sand ditch pattern was created.
- Qualitative analysis of the various factors' influence on the infiltration rate(i).
- There is turning point '*t0*' in the change curve of '*i*' with '*t*', and established a model of '*t0*'.
- Established a model of '*i*'.
- The models were validated by experimental data, and the prediction effect was good.

ABBREVIATIONS AND SYMBOLS

K_{ss}	Sand ditch soil saturated hydraulic conductivity
K_{so}	Original homogenous fine-textured soil saturated hydraulic conductivity
W	Sand ditch width
S	Sand ditch spacing
D	Sand ditch depth
SDCS	Sand ditch coarse-textured soil
OHFS	Original homogeneous fine-textured soil
γ	Bulk density
i	Soil infiltration rate (cm/min)
I	Cumulative infiltration (mL)
A	Soil area (cm^2)
θ	Soil water content (cm^3/cm^3)
t	Time (min)
$K(h)$	Unsaturated hydraulic conductivity (cm /min)
h	Soil water pressure head (cm)
x	Horizontal coordinate (cm)
z	Vertical coordinate (cm)
K_s	Saturated hydraulic conductivity (cm/min)
S_e	Effective degree of saturation

a	Empirical parameter
n and m	Empirical parameters affecting the shape of the soil water retention curve (m = 1 – 1/n)
t_0	Turning point of soil infiltration rate curve under banded sand ditch pattern (min)
RMSE	Root mean square error
NSE	Nash Sutcliffe efficiency
Mi and *Si*	Observed and predicted values, respectively
M_m	Mean of observed data
N	Total number of observations
CLM	Clay loam*
SLM	Silt loam*
LM1	Loam*
LM2	Loam**
LM3	Loam***
LSD	Loamy sand*
SD1	Sand****
SD2	Sand***
δ	Penetration enhancement rate

INTRODUCTION

Global climate change and intense human activities have made global water security issues increasingly prominent. As a result, society is facing increasingly serious water problems such as water shortages, water pollution, floods, droughts, and other related crises (Abbaspour *et al.* 2015; Pan *et al.* 2019). With increased urbanization, which is an important symbol of human social development, water safety has aroused widespread concern from all social classes (Wang & Zhang 2019; Keya & Aysha 2021). With the rapid expansion of urban areas, the original landscape of infiltration underlying the surface (woodland and grassland) is replaced by hardened ground. This phenomenon causes a series of ecological and environmental problems such as impeding rainfall infiltration, increasing surface runoff, urban waterlogging, soil drying, and groundwater-level decline. To reduce the impact of urban construction on the environment, it is necessary to fully utilize urban rainwater resources.

Many countries and regions have introduced the construction of a 'sponge city' with natural accumulation, penetration, and purification, which encourages the development of low-impact technologies, such as sponge roads, rain gardens, recessed green spaces, constructed wetlands, and green roofs so that rainwater can be absorbed and utilized on the spot. For local rainwater absorption, the role of the infiltration effect of vegetation, soil, and other natural underlying surfaces is important to maximize the conversion of rainwater into soil water. This process mainly depends on rainfall intensity and the soil infiltration rate. In a single rainfall event, it is impossible to artificially control rainfall intensity and improvement of the rainwater local absorption rate can only be achieved by increasing the soil infiltration rate.

Infiltration characteristics are a fixed property of soil that determines the efficiency of rainwater conversion into soil water. The main factor affecting the soil infiltration rate is soil texture. Furthermore, soil bulk density and soil configuration have a significant impact on soil infiltration characteristics. It was previously determined that setting sand ditches in weak permeability soil enhances water infiltration. Abu-Zreig *et al.* (2000) and Abu-Zreig & Tamimi (2011) experimented with sand ditch rainfall collection and found that sand ditches can effectively collect rainwater, intercept runoff, reduce sediment transport, prolong the peak reach time, and improve crop production for dry landscapes. Widomski *et al.* (2010) evaluated the infiltration enhancement effect of a banded sand ditch in an orchard in Olszanka and observed that the infiltration rate of terraces equipped with sand-filled drains increased by an average of 12.6%. Abu-Zreig *et al.* (2020) confirmed that sand ditches increased water infiltration volume and soil moisture storage, especially in high-density soils, and the presence of sand ditches increased the rainwater infiltration volume by 156%. Barber *et al.* (2003) studied the effects of ecological ditches (composed of compost, sand, gravel, and perforated drainage pipes) on the peak delay time of urban rainstorms and simulated peak reduction. Ecological ditches can reduce the peak flow of rainstorms by 10–50%. The size of the ditch and media type are key factors for the peak delay time.

Due to the high infiltration rate of sand ditches, rainfall, and runoff can quickly enter the soil profile through the sand ditch to limit water evaporation and quickly store precipitation resources in deep soil, which help solve the water demand of plants in arid periods. Sand ditch rainfall harvesting technology provides an important method for alleviating the negative

hydrological impact of urbanization. When applied to road green belts, urban road runoff, rain gardens, and green roofs in cities, these ditches increase the soil infiltration rate and cities obtain a higher rainwater adsorption rate. This has a major impact on solving the water shortage problem in the hydropenia season and flood problems in the rainy season. Therefore, to thoroughly implement sand ditch technology in urban rainwater management, reasonably set sand ditch parameters, and avoid unnecessary consumption of human and financial resources, it is necessary to quantitatively analyze the change of the soil infiltration rate after setting sand ditches. Numerical simulation is an effective method for the analysis of a large amount of data. HYDRUS can be used to simulate the infiltration process of water in different layers of soil under different water accumulation conditions (Šimůnek *et al.* 2018). Wang *et al.* (2014) simulated and analyzed the infiltration characteristics of fine soil with a coarse sand interlayer under the conditions of pounding rainfall with HYDRUS software, and the grainy sand interlayer with higher matrix suction promoted rather than inhibited soil infiltration. Sasidharan *et al.* (2020) used HYDRUS software to conduct a numerical simulation and compared the groundwater recharge effects of drywall (DWS) and infiltration bases (IBS) on the penetration of tight clay layers. The authors found that drywall facilitates the rapid infiltration and recharge better than infiltration bases. Hilten *et al.* (2008) and Xie *et al.* (2019) evaluated the effect of green roofing on rainwater runoff with the help of the HYDRUS simulation. Saito *et al.* (2012) utilized experimental results to confirm that HYDRUS can reliably simulate soil water movement in sand ditches and evaluated the water storage capacity of sandy ditches.

Based on the HYDRUS model, this paper choose the soil water movement equation and defined the solution conditions under a banded sand ditch pattern. The effects of soil parameters (sand ditch coarse-textured soil (SDCS) and original homogeneous fine-textured soil (OHFS)) and sand ditch structural parameters (sand ditch spacing (S), sand ditch width (W), sand ditch depth (D)) on the soil infiltration rate were simulated. This simulation data was used to analyze the influence degree of five factors on the soil infiltration rate. Then, the calculation model of the soil infiltration rate was established. The reliability of the calculation model was verified through laboratory experiments.

MATERIALS AND METHODS

Soil tank laboratory experiments

The laboratory test was used to evaluate the reliability of the soil infiltration rate prediction model under a banded sand ditch pattern. The tested loam and fine sand were from Jingtai County, Baiyin City, China, and the silty loam and coarse sand were from Qilihe District, Lanzhou City. The soil was collected from 0 to 40 cm underground. Soils used for the experiment were air-dried, rolled, uniformly mixed, and sieved through a 2 mm sieve. The bulk density (γ) of the soil used in the experiment was determined by a ring knife method, and the soil saturated hydraulic conductivity was measured using the constant head method.

Figure 1 illustrates the equipment for the laboratory experiments, and Figure 2 shows the device diagram of a laboratory experiment. The experimental device consists of four parts as follows: an adjustable bracket, a soil tank, a water supply system, and a drainage system. The water supply system is composed of a water bucket, inlet pipe, peristaltic pump, and outlet pipe; the drainage system consists of an outflow pipe and a measuring cylinder. Both soil tanks are composed of 10 mm thick plexiglass bonds, and the internal dimensions of the two soil tanks are $30 \times 10 \times 100$ cm and $40 \times 10 \times 100$ cm (length $\times$ width $\times$ height). Vent holes occur at the bottom of the soil tank at 2 mm diameter to prevent air resistance during infiltration. The diameter of the water bucket was 10 cm and the height was 100 cm. The outflow pipe inlet was set 2 cm above the soil surface to maintain a constant 2 cm head on the soil surface during infiltration.

Considering SDCS, OHFS, *S*, *W* and *D* factors, four groups of laboratory experiments were designed and test schemes are shown in Table 1. First, the air-dried fine-textured soil was loaded into soil tanks in layers according to the soil bulk density. To prevent the sidewall soil from collapsing, the original soil was supported with a thin metal plate and sand was loaded into the sand ditch in layers according to the bulk density. The thickness of each soil layer was 5 cm and a roughening treatment was conducted between layers. Finally, the metal plate was slowly pulled up. The soil box filled with soil samples was deposited for 24 h and then the testing began. Water was added to the predetermined 2 cm constant head at the beginning of the test. Moreover, the peristaltic pump was switched to supply water according to the set flow rates (q) and the excess water flowed out into the measuring cylinder. During experiments, cylinder data were recorded at the predetermined time until infiltration was stable. Table 1 shows design schemes of the laboratory experiments.

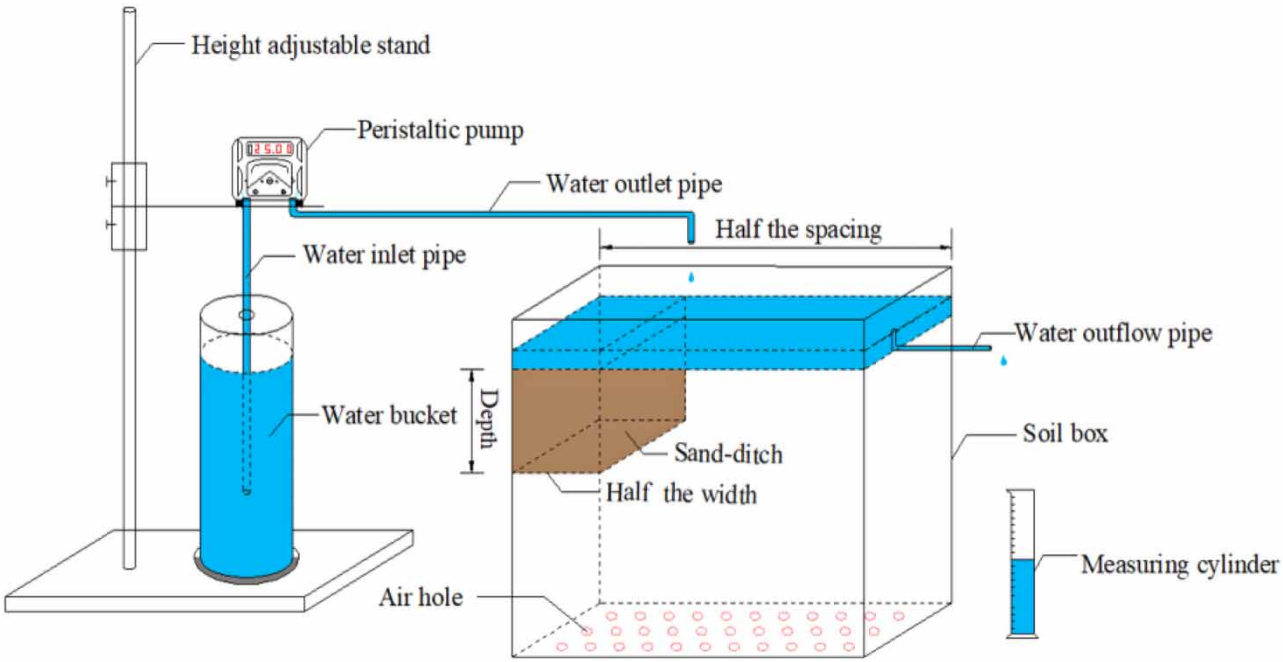

Figure 1 | Diagram of soil tank experimental equipment.

Figure 2 | The device diagram of laboratory experiment.

Calculated soil infiltration rate by cumulative infiltration.

$$i = \frac{dI}{Adt} \tag{1}$$

where i is the soil infiltration rate (cm/min), I is the cumulative infiltration (mL), A is the soil area (cm^2), and t is the time (min).

Table 1 | Verification test parameters of sand ditches infiltration rate calculation formula

Treatment	SDCS (K_s (cm/min))	OHFS (K_s (cm/min))	S (cm)	W (cm)	D (cm)
T1	0.274	0.0187	60	10	20
T2	0.646	0.0216	80	14	30
T3	0.554	0.011	70	12	25
T4	0.225	0.017	50	14	20

In any period when the predetermined flow rate is greater than the soil infiltration rate, part of the water provided by the peristaltic pump will penetrate the soil (marked as I) and the other part of the water that has not penetrated the soil will flow into the measuring cylinder (marked as L). According to the principle of water balance, the accumulated infiltration amount in the soil can be obtained according to Equation (2).

$$I = V - L \tag{2}$$

where V is the amount of water supplied by the peristaltic pump (mL), and L is the water volume in the measuring cylinder (mL).

Numerical simulations

The soil infiltration rates can be simulated under the banded sand ditch model using HYDRUS-2D. The governing equation for water flow is the 2D Richards equation (Richards 1931), which can be described as follows:

$$\frac{\partial \theta}{\partial t} = \frac{\partial}{\partial x}\left[K(h)\frac{\partial h}{\partial x}\right] + \frac{\partial}{\partial z}\left[K(h)\frac{\partial h}{\partial z} + K(h)\right] \tag{3}$$

where θ is the soil water content (cm^3/cm^3), t is time (min), $K(h)$ is the unsaturated hydraulic conductivity (cm/min), h is the soil water pressure head (cm), x is the horizontal coordinate (cm), and z is the vertical coordinate and is positive upward (cm).

The van Genuchten-Mualem (Mualem 1976; van Genuchten 1980) constitutive relationships were used to describe soil hydraulic characteristics provided as follows:

$$\theta(h) = \begin{cases} \theta_r + \dfrac{\theta_s - \theta_r}{(1 + |\alpha h|^n)^m} & h < 0 \\ \theta_s & h \geq 0 \end{cases} \tag{4}$$

$$K(h) = K_s S_e^{1/2}[1 - (1 - S_e^{1/m})^m]^2 \tag{5}$$

where $S_e = \theta - \theta_r / \theta_s - \theta_r$, $m = 1 - \dfrac{1}{n}$, $n > 1$.

where θ_r is the residual water content (cm^3/cm^3), θ_s is the saturated water content (cm^3/cm^3), K_s is the saturated hydraulic conductivity (cm/min), S_e is the effective degree of saturation, α is an empirical parameter (1/cm), and m and n are empirical constants (–).

Figure 3 shows the structure of the soil profile in the banded sand ditch pattern. Sand ditches of the same width and depth are arranged in parallel with the same interval. Therefore, this is an axisymmetric two-dimensional plane problem. Considering the symmetry of the sand ditch, half of the control area of the sand ditch was selected as the simulation area (Figure 4). The initial matrix of test soils are used as the initial conditions. In most cases, rainwater cannot infiltrate and there will be a thin layer of water on the upper boundary of the soil where the constant head is set ($h = 2$ cm). Free drainage BC was used along the bottom boundary without the influence of groundwater and rainfall. The contact boundary between sand and the original soil is not affected by the outside and so it is set as a free drainage BC and a no-flux boundary for all remaining boundaries. When solving, the Galerkin finite element method was used to disperse the soil profile in space, and the implicit difference scheme was used to disperse the profile in time; the simulated soil depth was 100 cm, the time step was 0.1 min, the space step was 1 cm, and the total simulation time was 120 min.

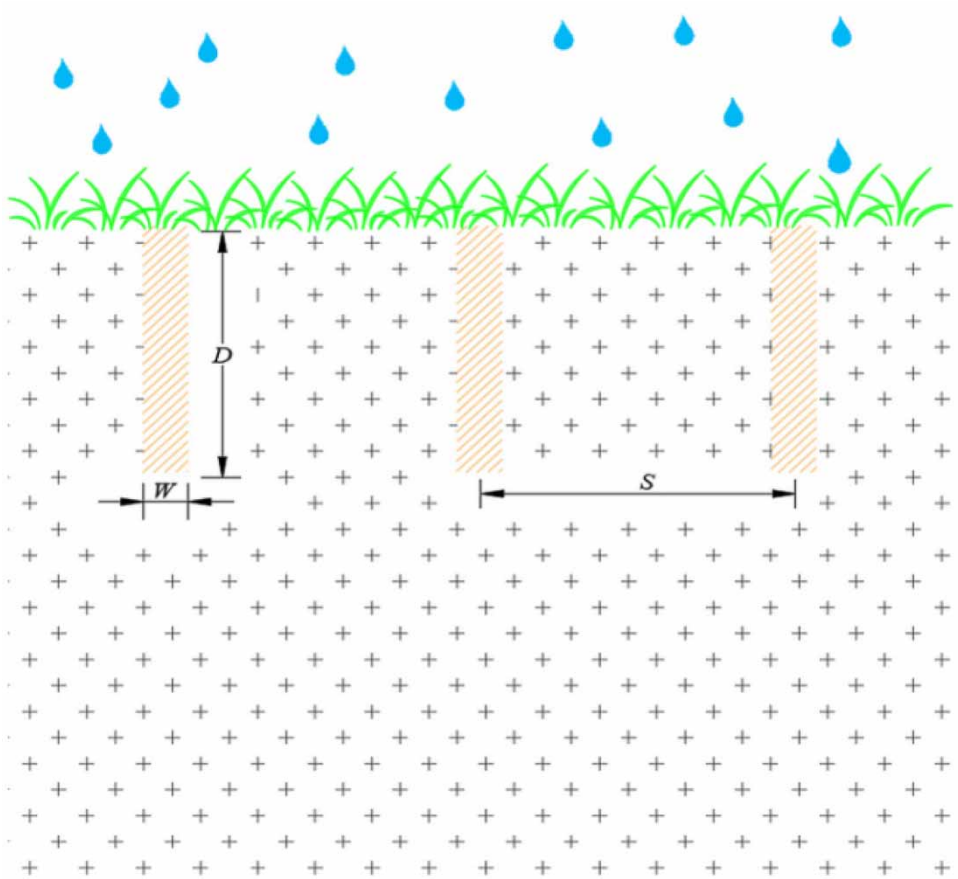

Figure 3 | Schematic diagram of sand ditch soil profile. *W* delegate sand-ditch width; *D* delegate sand-ditch depth; *S* delegate sand-ditch spacing.

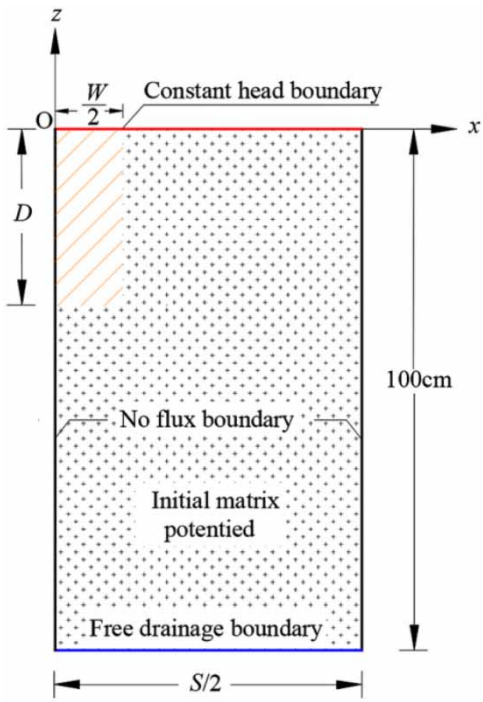

Figure 4 | Sketch map of solving region. *W* delegate sand-ditch width; *D* delegate sand-ditch depth; *S* delegate sand-ditch spacing.

Simulation scheme

To establish a soil infiltration rate prediction model of banded sand ditches that is more applicable and truly reflects the infiltration process, 10 soil parameters from the published literature were used for numerical simulation and five of these soils were selected from waterlogged cities (Carsel & Parrish 1988; Young *et al.* 2002; Ma *et al.* 2011; Fan *et al.* 2016; Li *et al.* 2018). The parameters of the 10 soils (VG-M) are listed in Table 2.

To set reasonable simulation schemes, the appropriate size range of the sand ditch is selected according to the existing data (Abu-Zreig & Tamimi 2011; Abu-Zreig *et al.* 2020; Saito *et al.* 2012). Combinations of 10 types of soil (Table 3), 5 types of spacing ($S = 40$, 50, 60, 70, and 80 cm), 5 widths ($W = 6$, 8, 10, 12, and 14 cm), and 5 depths ($D = 10$, 15, 20, 25, and 30 cm) were used to form 51 groups of simulation schemes. These designs included 5 groups of original soil infiltration contrast schemes without a sand ditch, 21 groups of single factor simulation schemes, which can be used to analyze single influencing factors, and 25 representative orthogonal simulation schemes. A total of 46 simulation scheme groups were used to explain the change of the soil infiltration rate under a banded sand ditch mode and these are listed in Table 3.

Statistical analysis

Using data processing software that handles data, the performance of the empirical model was assessed with the root mean square error (RMSE) and Nash-Sutcliffe efficiency (NSE) tests. If the results of the comparison show a RMSE that is close to 0 and a NSE that is close to 1, this indicates that the empirical model has good predictive performance. The statistical parameters are defined by the following equation (Moriasi *et al.* 2007):

$$\mathrm{RMSE} = \left[\frac{1}{N}\sum_{i=1}^{n}(M_i - S_i)^2\right]^{0.5} \tag{6}$$

$$\mathrm{NSE} = 1 - \frac{\sum_{i=1}^{n}(M_i - S_i)^2}{\sum_{i=1}^{n}(M_i - M_m)^2} \tag{7}$$

where M_i and S_i are the observed and predicted values, respectively, M_m is the mean of observed data, and N is the total number of observations.

RESULTS AND DISCUSSION

Analysis of factors influencing sand ditch infiltration rate

To illustrate the influence of single factors changing the original soil infiltration rate under the banded sand ditch pattern, the numerical simulation results of 21 groups of single factor schemes were used for analysis.

Table 2 | Van Genuchten-Mualem model parameters of ten typical soils

Soil texture	Shortened as	θ_r ($cm^3 \cdot cm^{-3}$)	θ_s ($cm^3 \cdot cm^{-3}$)	α (cm^{-1})	n (-)	K_s ($cm \cdot min^{-1}$)
Clay loam*	CLM	0.095	0.410	0.019	1.31	0.0043
Silt loam*	SLM	0.067	0.450	0.020	1.41	0.0075
Loam*	LM1	0.078	0.430	0.036	1.56	0.0173
Loam**	LM2	0.000	0.350	0.005	1.36	0.0280
Loam***	LM3	0.050	0.372	0.012	1.68	0.0340
Loamy sand*	LSD	0.057	0.410	0.124	2.28	0.2432
Sand****	SD1	0.007	0.372	0.059	2.32	0.3240
Sand***	SD2	0.045	0.430	0.145	2.68	0.4950
Sand*****	SD3	0.080	0.455	0.015	1.45	0.7500
Sand***	SD4	0.009	0.385	0.081	2.68	1.6000

Note: * from the literature [Carsel & Parrish 1988]; ** from the literature [Ma *et al.* 2011]; *** from the literature [Fan *et al.* 2016]. **** from the literature [Young *et al.* 2002]; ***** from the literature [Li *et al.* 2018].

Table 3 | Simulation schemes

Simulation Scheme	SDCS	OHFS	*S* (cm)	*W* (cm)	*D* (cm)
1	LSD	LM1	50	10	20
2	SD1	LM1	50	10	20
3	SD2	LM1	50	10	20
4	SD3	LM1	50	10	20
5	SD4	LM1	50	10	20
6	SD2	CLM	50	10	20
7	SD2	SLM	50	10	20
8	SD2	LM2	50	10	20
9	SD2	LM3	50	10	20
10	SD2	LM1	40	10	20
11	SD2	LM1	60	10	20
12	SD2	LM1	70	10	20
13	SD2	LM1	80	10	20
14	SD2	LM1	50	6	20
15	SD2	LM1	50	8	20
16	SD2	LM1	50	12	20
17	SD2	LM1	50	14	20
18	SD2	LM1	50	10	10
19	SD2	LM1	50	10	15
20	SD2	LM1	50	10	25
21	SD2	LM1	50	10	30
22	LSD	CLM	40	6	10
23	LSD	SLM	50	8	15
24	LSD	LM1	60	10	20
25	LSD	LM2	70	12	25
26	LSD	LM3	80	14	30
27	SD1	CLM	50	10	25
28	SD1	SLM	60	12	30
29	SD1	LM1	70	14	10
30	SD1	LM2	80	6	15
31	SD1	LM3	40	8	20
32	SD2	CLM	60	14	15
33	SD2	SLM	70	6	20
34	SD2	LM1	80	8	25
35	SD2	LM2	40	10	30
36	SD2	LM3	50	12	10
37	SD3	CLM	70	8	30
38	SD3	SLM	80	10	10
39	SD3	LM1	40	12	15
40	SD3	LM2	50	14	20
41	SD3	LM3	60	6	25
42	SD4	CLM	80	12	20

(*Continued.*)

Table 3 | Continued

Simulation Scheme	SDCS	OHFS	S (cm)	W (cm)	D (cm)
43	SD4	SLM	40	14	25
44	SD4	LM1	50	6	30
45	SD4	LM2	60	8	10
46	SD4	LM3	70	10	15

Influence of soil texture

Under conditions of $S = 50$ cm, $W = 10$ cm, and $D = 20$ cm, the dynamic change process of the soil infiltration rate under different combinations of SDCS and OHFS is simulated and shown in Figure 5. To compare and analyze the infiltration characteristics of the banded sand ditch and the original homogeneous fine-textured soil, the original control soils without sand ditch infiltration rate curves were added to Figure 5(a) and 5(b).

Figure 5 shows that there is an obvious turning point in the soil infiltration rate curve in the banded sand ditch pattern that we defined as 't_0.' The values of 't_0' change with changes in SDCS and OHFS. During the infiltration process, the initial value of 'i' was relatively large. With increased time, 'i' rapidly decreases, and when the infiltration progresses to 't_0,' 'i' will rapidly decrease again and then gradually stabilize.

Figure 5(a) shows that when only changing the texture of OHFS, the more delicate the OHFS, the higher the penetration enhancement rate (δ) (defined as the percentage increase in 'i' in the banded sand ditch mode compared with 'i' in the same period without the sand ditch mode). For example, at the end of the simulation time (2 h) and when the original homogeneous soil CLM sets the sand ditch soil conditions of SD2 as $S = 50$ cm, $W = 10$ cm, and $D = 20$ cm, 'δ' is 102%; in contrast, LM3 has relatively lower clay content under the same conditions and 'δ' is only 19.8%. This is because when the water infiltration starts, water simultaneously moves into the SDCS and OHFS, but because the saturated hydraulic conductivity (K_{ss}) of SDCS is large, the SDCS will soon saturate. While the saturated hydraulic conductivity (K_{so}) of OHFS is small, the wet front moves slow and in a short time it is unable to reach the bottom of the sand ditch. Thus, a lateral seepage surface appears at the interface between the sand ditch and the original soil (the size of the seepage surface is the sum of the width of the sand ditch and the depth of the sand ditch minus the OHFS wet front migration distance) and causes the SDCS water to move through the lateral seepage surface in the OHFS. The finer the texture of OHFS, the smaller the K_{so} and the slower the migration speed of the wet front, the larger the lateral seepage surface, the greater the lateral seepage volume, and the more

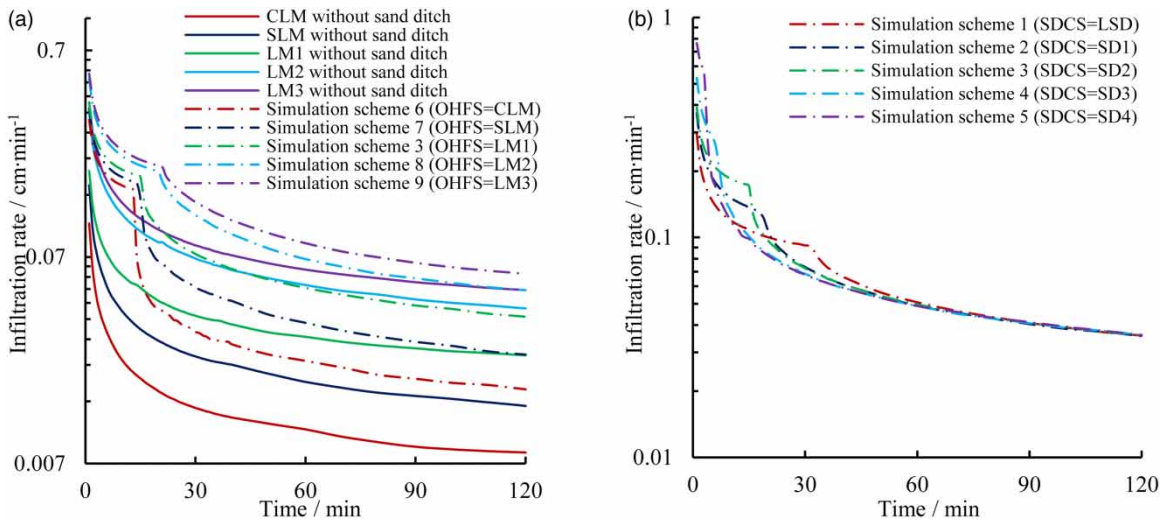

Figure 5 | Variation diagram of soil infiltration rate by changing the texture of original soil or sandy soil under the condition of the same sand ditch size. (a) Variation of soil infiltration rate before and after adding sand ditch for different original soil texture. (b) Variation of soil infiltration rate under different sandy soil texture.

obvious the effect of improving permeability. In addition to the above phenomena, the effects of OHFS on 't_0' are all manifested when there is a greater clay content in OHFS. In addition, the smaller 't_0' is because before the water reaches the bottom of the sand ditch and while the water infiltrates rapidly in the vertical direction in the SDCS, it also infiltrates laterally to the OHFS. The higher the soil clay content, the weaker the water conductivity and the less water can penetrate the OHFS from the SDCS side, and the SDCS becomes easy to saturate.

Figure 5(b) shows that when OHFS, *S*, *W*, and *D* are fixed, the higher the sand content of SDCS and the smaller 't_0.' For example, in LM1 with the SD2 ditch and LM1 with SD4, 't_0' is 15 and 3 min, respectively, because the higher the sand content in the SDCS, then the larger K_{ss}, the faster the water migration in the SDCS, and the shorter the time required for water to reach the bottom of the sandy ditch. The influence of SDCS on '*i*' mainly occurs before 't_0.' The higher the sand content of SDCS, the greater the initial value of '*i*.' For example, in the first minute of infiltration (for LM1 with the LSD ditch), the value of '*i*' is only 0.294 cm/min, while for the case of LM1 with the SD4 ditch, '*i*' increases to 0.764 cm/min. After infiltration reaches 't_0,' then '*i*' rapidly decreases. The higher the sand content of SDCS, the faster the decay of '*i*.' When time reaches 70 minutes, the influence of the SDCS texture type on '*i*' is weakened and its value stabilizes because after the water reaches the bottom of the sand ditch and it becomes saturated, then it cannot increase infiltration by storing excess water and can only increase the infiltration of the OHFS through the lateral seepage surface, which results in a rapid decrease in 'δ.' As time passes, the OHFS wetting front reaches the bottom of the sand ditch and the lateral seepage surface disappears. Infiltration in the banded sand ditch pattern is transformed into a vertical one-dimensional infiltration in OHFS, and the texture type of SDCS has no effect on '*i*.'

Influence of sand ditch parameters

Figure 6 shows the variation in the soil infiltration rate under the banded sand ditch pattern, which is under the constant soil conditions of LM1 with the SD2 ditch by changing the sand ditch structure (the size of parameters *S*, *W*, and *D*).

Figure 6 shows that like the influence of SDCS and OHFS on '*I*,' 't_0' also exists under the influence of sand ditch structure parameters (*S*, *W*, and *D*). Using 't_0' as the boundary, '*i*' has a rapid decline in two time periods and gradually stabilizes. Figure 6(a) shows that *S* does not affect 't_0.' In the case of LM1 with the SD2 ditch ($W = 10$ cm and $D = 20$ cm), the 't_0' values corresponding to different '*S*' values (40, 50, 60, 70, and 80 cm) are all 15 min. Furthermore, as '*S*' increases both '*i*' and 'δ' decrease. The reason is that under certain *W* conditions, the increase in *S* indirectly reduces the proportion of sand ditches in the soil profile (*W*/*S*) and thereby weakens the extreme permeability of the sand ditch. In addition, the wider the '*W*,' the weaker the influence of lateral infiltration of water in the sand ditch on vertical infiltration and the shorter the time for water to reach the bottom of the sand ditch. As '*D*' increases, 't_0' also gradually increases while '*i*' and 'δ' also significantly increase (Figure 6(c)). The reason is that as '*D*' becomes deeper, then it takes for the water to reach the bottom of the sandy ditch. In addition, as '*D*' becomes deeper, the larger the lateral contact surface between the sand ditch and the original soil, the greater the amount of lateral infiltration of water in the sand ditch, and the more noticeable the effect of increasing infiltration.

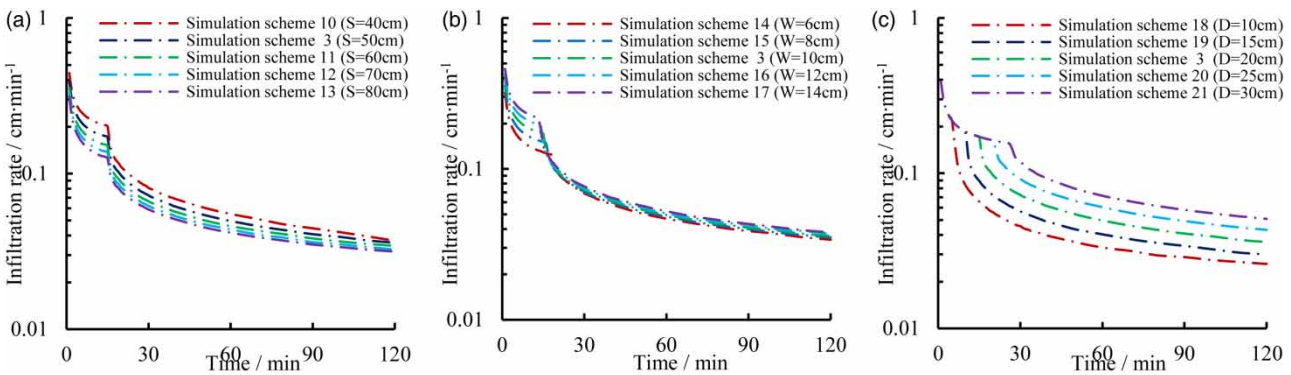

Figure 6 | Variation of soil infiltration rate by changing the size of sand ditch under the same soil combination. (a) Variation of soil infiltration rate under different sand ditch spacing. (b) Variation of soil infiltration rate under different sand ditch width. (c) Variation of soil infiltration rate under different sand ditch depth.

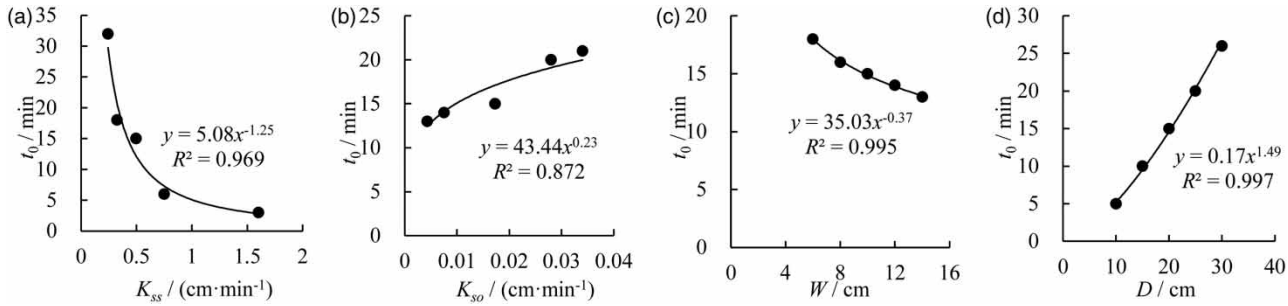

Figure 7 | The relationship between t_0 and various influencing factors. (a) $K_{so} = 0.0173$ cm/min, $W = 10$ cm, $D = 20$ cm, $S = 60$ cm. (b) $K_{ss} = 0.495$ cm/min, $W = 10$ cm, $D = 20$ cm, $S = 60$ cm. (c) $K_{ss} = 0.495$ cm/min, $K_{so} = 0.0173$ cm/min, $D = 20$ cm, $S = 60$ cm. (c) $K_{ss} = 0.495$ cm/min, $K_{so} = 0.0173$ cm/min, $W = 10$ cm, $S = 60$ cm.

Predictive model establishment of 't_0'

The saturated hydraulic conductivity of the soil is affected by the soil texture and plays an important role in the engineering design of irrigation and drainage systems. To simplify the construction of the model, K_{ss} and K_{so} are utilized to characterize the coarse-textured soil and the original homogeneous fine-textured soil difference. The sensitivity analysis of the five factors that may affect 't_0' and the results show that the values of 'P' for K_{ss}, K_{so}, and D are less than 0.01, which indicates that these factors have a significant impact on 't_0.' The effect of 'S' is small ($P = 0.13$) and can be ignored. The influence degree of each factor is '$K_{ss} > D > K_{so} > W$.' To quantitatively analyze the functional relationship between 't_0' and 'K_{ss}, D, K_{so}, and W,' except for the factors to be analyzed, other factors are controlled so that they remain unchanged and a trend chart of 't_0' is created under the influence of this factor (Figure 7).

As shown in Figure 7, there is a good power function relationship between each factor and 't_0,' and the power function multiplication form can be used to establish the 't_0' prediction model. The expression is described as follows:

$$t_0 = a_0 K_{ss}^{a_1} K_{so}^{a_2} W^{a_3} D^{a_4} \tag{8}$$

where t_0 is the turning point of the soil infiltration rate curve under the banded sand ditch pattern (min), a_0 is a coefficient, and a_1, a_2, a_3, and a_4 are the exponents.

Based on numerical results of 46 sets of simulation schemes (Table 4) and the fitting Equation (8), the coefficient a_0 is 1.05 and the exponents $a_1 \sim a_4$ are -1.00, 0.22, -0.46, and 1.31, respectively. Furthermore, the 't_0' prediction model under different K_{ss}, K_{so}, W, and D conditions is obtained as follows.

$$t_0 = 1.05 K_{ss}^{-1.00} K_{so}^{0.22} W^{-0.46} D^{1.31} \quad (R^2 = 0.958) \tag{9}$$

Model assessment

Using numerical simulation data to evaluate the simplified prediction model that characterizes 't_0,' we compared and analyzed the calculated value of the simplified prediction model with the numerical simulation value. The comparison result is shown in Figure 8.

Figure 8 shows that points of the 't_0' simulated value and the model-calculated value coordinates are distributed and are near the 1:1 line, which indicates that the correlation is good and is used to calculate the error-index parameters. The RMSE is 2.07 min and the NSE value is 0.962, which indicates that the 't_0' prediction model has good accuracy. The significance of the model is to estimate the time when water reaches the bottom of the sand ditch to build a more accurate prediction model of 'i.'

CONSTRUCTION AND VERIFICATION OF THE SOIL INFILTRATION RATE MODEL

Description of the soil infiltration rate

According to the previous analysis, the infiltration rate changes before and after 't_0' are inconsistent. Using 't_0' as the boundary, the soil infiltration rate changes under this model are divided into two stages. The Kostiakov infiltration formula

Table 4 | The values of parameters α and β are obtained by formula fitting in each group of experiments

Treatment	K_{ss}	K_{so}	S	W	D	t_0	β_1	ε_1	R^2	β_2	ε_2	R^2
1	0.2432	0.0173	50	10	20	32	0.27	0.34	0.976	0.75	0.65	0.983
2	0.324	0.0173	50	10	20	18	0.35	0.37	0.989	0.66	0.64	0.974
3	0.495	0.0173	50	10	20	15	0.37	0.31	0.980	0.72	0.66	0.968
4	0.75	0.0173	50	10	20	6	0.53	0.39	0.998	0.64	0.65	0.961
5	1.6	0.0173	50	10	20	3	0.76	0.29	0.998	0.53	0.61	0.969
6	0.495	0.0043	50	10	20	13	0.31	0.31	0.977	0.25	0.60	0.961
7	0.495	0.0075	50	10	20	14	0.35	0.32	0.979	0.55	0.69	0.965
8	0.495	0.028	50	10	20	20	0.49	0.35	0.989	1.27	0.71	0.987
9	0.495	0.034	50	10	20	21	0.52	0.35	0.990	1.32	0.67	0.988
10	0.495	0.0173	40	10	20	15	0.42	0.30	0.979	0.80	0.66	0.984
11	0.495	0.0173	60	10	20	15	0.34	0.32	0.980	0.59	0.63	0.967
12	0.495	0.0173	70	10	20	15	0.32	0.34	0.982	0.51	0.61	0.968
13	0.495	0.0173	80	10	20	15	0.30	0.35	0.983	0.45	0.59	0.970
14	0.495	0.0173	50	6	20	18	0.31	0.33	0.981	0.61	0.63	0.972
15	0.495	0.0173	50	8	20	16	0.34	0.32	0.980	0.68	0.65	0.965
16	0.495	0.0173	50	12	20	14	0.41	0.30	0.981	0.69	0.64	0.977
17	0.495	0.0173	50	14	20	13	0.44	0.30	0.981	0.80	0.68	0.971
18	0.495	0.0173	50	10	10	5	0.39	0.37	0.995	0.40	0.65	0.94
19	0.495	0.0173	50	10	15	10	0.38	0.33	0.989	0.52	0.64	0.967
20	0.495	0.0173	50	10	25	20	0.37	0.29	0.974	0.85	0.65	0.978
21	0.495	0.0173	50	10	30	26	0.36	0.28	0.969	1.05	0.65	0.983
22	0.2432	0.0043	40	6	10	11	0.19	0.39	0.987	0.20	0.67	0.946
23	0.2432	0.0075	50	8	15	22	0.22	0.36	0.981	0.61	0.58	0.964
24	0.2432	0.0173	60	10	20	32	0.24	0.32	0.982	0.56	0.60	0.986
25	0.2432	0.028	70	12	25	40	0.36	0.38	0.991	1.05	0.63	0.989
26	0.2432	0.034	80	14	30	50	0.39	0.37	0.990	0.81	0.52	0.974
27	0.324	0.0043	50	10	25	23	0.28	0.36	0.956	0.31	0.59	0.976
28	0.324	0.0075	60	12	30	31	0.29	0.32	0.976	0.83	0.69	0.985
29	0.324	0.0173	70	14	10	9	0.38	0.37	0.920	0.21	0.58	0.990
30	0.324	0.028	80	6	15	22	0.38	0.31	0.997	0.48	0.62	0.993
31	0.324	0.034	40	8	20	29	0.32	0.37	0.993	0.91	0.67	0.992
32	0.495	0.0043	60	14	15	8	0.34	0.32	0.986	0.18	0.60	0.945
33	0.495	0.0075	70	6	20	17	0.23	0.35	0.979	0.32	0.59	0.965
34	0.495	0.0173	80	8	25	22	0.26	0.31	0.979	0.51	0.58	0.973
35	0.495	0.028	40	10	30	37	0.48	0.29	0.984	4.13	0.71	0.973
36	0.495	0.034	50	12	10	7	0.56	0.35	0.994	0.53	0.51	0.985
37	0.75	0.0043	70	8	30	11	0.30	0.36	0.988	0.22	0.53	0.950
38	0.75	0.0075	80	10	10	3	0.37	0.38	0.941	0.35	0.81	0.990
39	0.75	0.0173	40	12	15	5	0.71	0.36	0.939	0.42	0.57	0.995
40	0.75	0.028	50	14	20	8	0.77	0.37	0.977	1.14	0.71	0.992
41	0.75	0.034	60	6	25	18	0.54	0.35	0.996	1.01	0.60	0.997
42	1.6	0.0043	80	12	20	3	0.53	0.30	0.997	0.15	0.56	0.956

(*Continued.*)

Table 4 | Continued

Treatment	K_{ss}	K_{so}	S	W	D	t_0	β_1	ε_1	R^2	β_2	ε_2	R^2
43	1.6	0.0075	40	14	25	4	1.12	0.25	0.992	0.67	0.69	0.934
44	1.6	0.0173	50	6	30	7	0.55	0.27	0.988	0.75	0.61	0.978
45	1.6	0.028	60	8	10	3	0.72	0.40	0.998	0.43	0.52	0.997
46	1.6	0.034	70	10	15	3	0.84	0.38	0.925	0.57	0.53	0.995

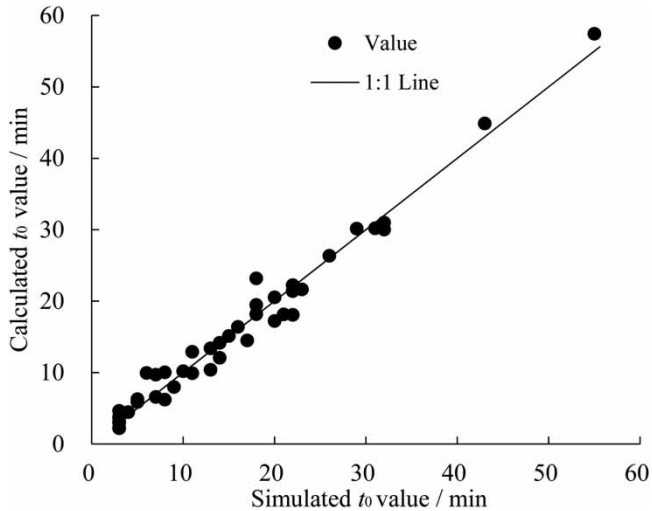

Figure 8 | Correlation diagram between the calculated value of the 't_0' model and the software simulated value.

(Kostiakov 1932) quantitatively describes the change process of the soil infiltration rate at each stage with time expressed as shown in Equation (10):

$$i = \begin{cases} \beta_1 \cdot t^{-\varepsilon_1} t \le t_0 \\ \beta_2 \cdot t^{-\varepsilon_2} t > t_0 \end{cases} \tag{10}$$

where i is the soil infiltration rate (cm/min), β_1 and β_2 are infiltration coefficients, and ε_1, ε_2 are infiltration exponents.

Determination of model parameters for the soil infiltration rate in banded sand ditches

Using a significance analysis of each influencing factor, it was concluded that during the $t \le t_0$ stage, each factor's influence degree of 'i' can be described as '$K_{ss} > W + S > K_{so} > D$'. Furthermore, '$K_{ss}$' and '$W$' have a significant impact on 'i.' Similarly, during the $t > t_0$ stage, each factor's influence degree for 'i' can be described as '$K_{so} > D + S > K_{ss} > W$,' and '$K_{so}$' and '$D$' have a significant impact on 'i'. Using Equation (10) and considering 't_0' as the demarcation, 46 sets of simulation plans (Table 3) are applied to the recursion data fitting to calculate the infiltration rate versus time. Then, values of β_1, β_2, ε_1, ε_2, and R^2 are obtained and results are shown in Table 4.

Table 4 shows that the coefficient of determination of the regression line fitted by all simulation schemes is close to 1 ($R^2 \ge 0.96$). These results indicate a good quantitative relationship between the infiltration rate and various influencing factors, and the Kostiakov infiltration formula can be used to quantitatively describe the change in the soil infiltration rate with time under a banded sand ditch pattern. The ε_1 and ε_2 exponent values show a small fluctuation range around their average value. Regarding results of the parameter sensitivity analysis, slight fluctuations in the values of 'ε_1' and 'ε_2' have little effect on the infiltration rate. To simplify this calculation, the average values of fitting parameters ε_1 and ε_2 can be used (0.33 and 0.65. respectively) to fix them. However, values of β_1 and β_2 greatly fluctuate. In this case, the average value cannot simply be used as a fixed value and further analysis is needed.

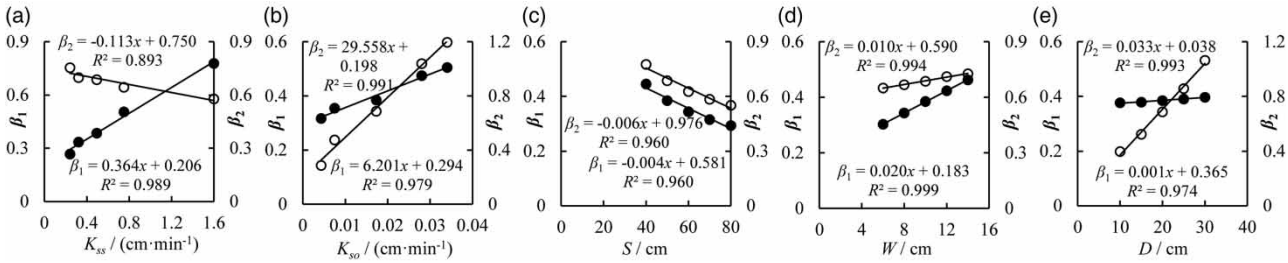

Figure 9 | The relationship between β_1, β_2 and various influencing factors. (a) $K_{so} = 0.0173$ cm/min, $W = 10$ cm, $D = 20$ cm, $S = 50$ cm. (b) $K_{ss} = 0.4950$ cm/min, $W = 10$ cm, $D = 20$ cm, $S = 50$ cm. (c) $K_{so} = 0.0173$ cm/min, $K_{ss} = 0.4950$ cm/min, $W = 10$ cm, $D = 20$ cm. (d) $K_{so} = 0.0173$ cm/min, $K_{ss} = 0.4950$ cm/min, $D = 20$ cm, $S = 50$ cm. (e) $K_{so} = 0.0173$ cm/min, $K_{ss} = 0.4950$ cm/min, $W = 10$ cm, $S = 50$ cm.

Construction of the soil infiltration rate model in the banded sand ditch pattern

Substituting $\varepsilon_1 = 0.34$ and $\varepsilon_2 = 0.63$ into Equation (10), using 't_0' as the demarcation point, and again fitting the numerical results of 46 sets of simulation schemes (Table 4), we can obtain new values of 'β_1' and 'β_2.' Next, quantitative analyses of the functional relationship between β_1, β_2, and K_{so}, K_{ss}, S, W, and D are shown in Figure 9.

Figure 9 shows that throughout the infiltration stage, K_{ss}, K_{so}, W, D, and S have a good linear relationship with β_1 and β_2.

The expression form is constructed for the infiltration rate coefficients β_1 and β_2 in the two time periods $t \le t_0$ and $t > t_0$ as follows:

$$\beta_1 = b_1 K_{ss} + b_2 K_{so} + b_3 S + b_4 W + b_5 D + b_0 \tag{11}$$

$$\beta_2 = c_1 K_{ss} + c_2 K_{so} + c_3 S + c_4 W + c_5 D + c_0 \tag{12}$$

where b_1, b_2, b_3, b_4, b_5, c_1, c_2, c_3, c_4, and c_5 are constant coefficients and b_0 and c_0 are constant values.

Furthermore, using Equations (11) and (12), the numerical results of 46 sets of simulation schemes (Table 4) are fitted to obtain $b_1 = 0.340$, $b_2 = 4.747$, $b_3 = -0.0046$, $b_4 = 0.0283$, $b_5 = 0.0019$, $b_0 = 0.07$; $c_1 = -0.075$, $c_2 = 23.871$, $c_3 = -0.003$, $c_4 = 0.0102$, $c_5 = 0.0247$, and $c_0 = -0.177$. By substituting the parameter values obtained by fitting into Equations (11) and (12), the specific expression form of β_1 and β_2 is as follows:

$$\beta_1 = 0.340 K_{ss} + 4.747 K_{so} - 0.0046 S + 0.0283 W + 0.0019 D + 0.07 \quad (R^2 = 0.830) \tag{13}$$

$$\beta_2 = -0.0745 K_{ss} + 23.871 K_{so} - 0.0029 S + 0.0102 W + 0.0247 D - 0.177 \quad (R^2 = 0.987) \tag{14}$$

In summary, the estimation model of the soil infiltration rate under the banded sand ditch pattern can be constructed as follows:

$$i = \begin{cases} (0.340 K_{ss} + 4.747 K_{so} - 0.0046 S + 0.0283 W + 0.0019 D + 0.07) \cdot t^{-0.34} & t \le t_0 \\ (-0.0745 K_{ss} + 23.871 K_{so} - 0.0029 S + 0.0102 W + 0.0247 D - 0.177) \cdot t^{-0.63} & t > t_0 \end{cases} \tag{15}$$

Model verification

To verify the reliability of the empirical model, Figure 10 shows that the calculated value of the estimated model is compared and analyzed with a measured value of the indoor test. The error analysis results are listed in Table 5.

Figure 10 shows that the calculated value agrees with the measured value. With Formula (6) and Formula (7), the estimation model is statistically analyzed and RMSE values are between 0.0085 and 0.0290 cm/min, which are close to 0, and the NSE value is between 0.824 and 0.989, which is close to 1. These results suggest that the model has a good prediction effect and can be used to estimate the soil infiltration rate under the banded sand ditches model. Moreover, the error mainly occurs in the advanced stage of infiltration (approximately at the stable infiltration stage), which is caused by the error of the Kostiakov formula used in this study. In addition, the Kostiakov formula is an empirical model with a simple form, which causes fitting results to be incompatible with measured values at the beginning and end. Specifically, the fitted infiltration

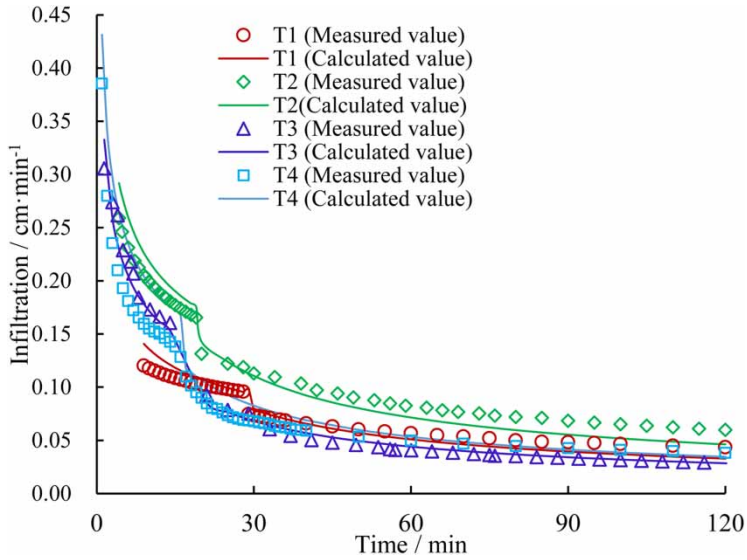

Figure 10 | Comparison of measured value and model calculated value.

Table 5 | Error analysis results

	T1	T2	T3	T4
RMSE	0.0085	00153	0.0088	0.0290
NSE	0.989	0.935	0.875	0.8240

rate is often too large at the initial moment of infiltration, and the fitted infiltration rate is lower than the measured value at the stage of stable infiltration.

CONCLUSIONS

Based on the HYDRUS model, a mathematical model of soil water movement under a banded sand ditch pattern was established, and 46 scenarios were set to numerically investigate the effects of soil texture parameters and sand ditch structure parameters on the soil infiltration rate under this pattern. When compared with the original homogeneous fine-textured soil infiltration process, the following conclusions were drawn from this information. The banded sand ditch shows a significant increase in the infiltration effect and there is a turning point 't_0' in the curve of the soil infiltration rate with time. In addition, 't_0' is not related to S but it increases with increasing K_{so} and D and decreases with increasing K_{ss} and W. Therefore, there is a determined power function relationship ($R^2 = 0.958$) between 't_0' and K_{ss}, K_{so}, D and W. The Kostiakov formula can be used to describe the infiltration process of banded sand ditch furrow soil. Because the Kostiakov formula has a small index change, the average values are 0.34 ($t \leq t_0$ stage) and 0.63 ($t > t_0$ stage) when determining the formula parameters. Coefficients of the Kostiakov formula and K_{ss}, K_{so}, W, S, and D satisfy the linear relationship. A model for estimating the soil infiltration rate under a banded sand ditch pattern was proposed, and the reliability of the model was verified by laboratory experiments (RMSE values are between 0.0085 and 0.0290 cm/min and the NSE value is between 0.827 and 0.989), which can be used to predict the soil infiltration rate under a banded sand ditch pattern. In this research, only five extremely important influencing factors (K_{ss}, K_{so}, W, S, and D) were analyzed when quantitatively describing the permeation effect under a sand ditch model and effects of rainfall intensity, soil bulk density, and soil initial moisture content on the soil infiltration rate under a sand ditch mode were not considered. Therefore, in future research, other influencing factors should be examined, which would improve the model established in this study and result in a more accurate description of the change process of the soil infiltration rate under a strip sand trench mode.

ACKNOWLEDGEMENTS

This research was supported by the National Natural Science Foundation of China (No. 51969013) and the National Natural Science Foundation of Gansu Province (No. 21JR7RA225).

DATA AVAILABILITY STATEMENT

All relevant data are included in the paper or its Supplementary Information.

REFERENCES

Abbaspour, K. C., Rouholahnejad, E. & Vaghefi, S. 2015 A continental-scale hydrology and water quality model for Europe: calibration and uncertainty of a high-resolution large-scale swat model. *Journal of Hydrology* **524**, 733–752. doi:10.1016/j.jhydrol.2015.03.027.

Abu-Zreig, M. & Tamimi, A. 2011 Field evaluation of sand-ditch water harvesting technique in Jordan. *Agricultural Water Management* **98** (8), 1291–1296. doi:10.1016/j.agwat.2011.03.008.

Abu-Zreig, M., Attom, M. & Hamasha, N. 2000 Rainfall harvesting using sand ditches in Jordan. *Agricultural Water Management* **46** (2), 183–192. doi:10.1016/S0378-3774(00)00082-2.

Abu-Zreig, M., Fujimaki, H. & Abd Elbasit, M. A. 2020 Enhancing water infiltration through heavy soils with sand-ditch technique. *Water* **12** (5), 1312. doi:10.3390/w12051312.

Barber, M. E., King, S. G., Yonge, D. R. & Hathhorn, W. E. 2003 Ecology ditch: a best management practice for storm water runoff mitigation. *Journal of Hydrologic Engineering* **8** (3), 111–122. doi:10.1061/ ~ ASCE!1084-0699 ~ 2003!8:3 ~ 111.

Carsel, R. F. & Parrish, R. S. 1988 Developing joint probability distributions of soil water retention characteristics. *Water Resources Research* **24** (5), 755–769. doi:10.1029/WR024i005p00755.

Fan, Y. W., Hang, N., Ma, X. Y., Bi, G. Q. & Zhao, W. J. 2016 Applying HYDRUS-1D to simulate the soil infiltration characteristics of sand interlayer. *Soils* **48** (001), 193–200. doi:10.13758/j.cnki.tr.2016.01.029.

Hilten, R. N., Lawrence, T. M. & Tollner, E. W. 2008 Modeling stormwater runoff from green roofs with hydrus-1d. *Journal of Hydrology* **358** (3), 288–293.

Keya, C. & Aysha, A. 2021 Water quality trend analysis in a citywide water distribution system. *Water Sci Technol* **84** (10–11), 3191–3210. https://doi.org/10.2166/wst.2021.342.

Kostiakov, A. N. 1932 On the dynamics of coefficient of water-percolation in soils and on necessity for studying it from a dynamic point of view for purposes of amelioration. In *Trans. 6th Comm. Intern. Soil Sci, Russia, Part A*, pp. 17–21.

Li, J., Zhao, R., Li, Y. & Chen, L. 2018 Modeling the effects of parameter optimization on three bioretention tanks using the hydrus-1d model. *Journal of Environmental Management* **217**, 38–46. doi:10.1016/j.jenvman.2018.03.078.

Ma, H., Yang, D. W. & Lei, H. M. 2011 Application and improvement of Hydrns-1D model for analyzing water cycle in an agricultural field. *Transactions of the CSAE* **27** (3), 6–12. doi:10.3969/j.issn.1002-6819.2011.03.002.

Moriasi, D. N., Arnold, J. G., Liew, M., Bingner, R. L., Harmel, R. D. & Veith, T. L. 2007 Model evaluation guidelines for systematic quantification of accuracy in watershed simulations. *Transactions of the Asabe* **50** (3), 885–900.

Mualem, Y. 1976 A new model for predicting the hydraulic conductivity of unsaturated porous media. *Water Resources Research* **12** (3), 513–522. doi:10.1029/WR012i003p00513.

Pan, P. H., Wang, Y. B. & Zhang, X. X. 2019 Emergency measure of soft isolation controlling pollution diffusion response to sudden water pollution accidents. *Water Sci Technol : A Journal of the International Association on Water Pollution Research* **80** (7), 1238–1248. doi:10.2166/wst.2019.368.

Richards, L. A. 1931 Capillary conduction of liquids through porous mediums. *Physics* **1** (5), 318–333. doi:10.1063/1.1745010.

Saito, T., Yasuda, H., Fujimaki, H., Inosako, K. & Abe, Y. 2012 Numerical calculation of soil water movement in a water harvesting system with sand ditches using hydrus-2d. *Journal of Arid Land Studies* **22** (1), 215–218.

Sasidharan, S., Bradford, S. A., Imnek, J. & Kraemer, S. R. 2020 Comparison of recharge from drywells and infiltration basins: a modeling study. *Journal of Hydrology* **594** (4), 125720. doi:10.1016/j.jhydrol.2020.125720.

Šimůnek, J., Van Genuchten, M. T. & Šejna, M. 2018 *The HYDRUS Software Package for Simulating the two-and Three-Dimensional Movement of Water, Heat, and Multiple Solutes in Variably-Saturated Media*. Technical manual, version 3.0. PC Progress, Prague, Czech Republic, pp. 274.

Van Genuchten, M. T. 1980 A closed-form equation for predicting the hydraulic conductivity of unsaturated soils. *Soil Science Society of America Journal* **44** (5), 892–898. doi:10.2136/sssaj1980.03615995004400050002x.

Wang, H. & Zhang, Q. 2019 Research advances in identifying sulfate contamination sources of water environment by using stable isotopes. *International Journal of Environmental Research and Public Health* **16** (11), 1914–1926. doi:10.3390/ijerph16111914.

Wang, C., Mao, X. & Hatano, R. 2014 Modeling ponded infiltration in fine textured soils with coarse interlayer. *Soil Science Society of America Journal* **78** (3), 745–753. doi:10.2136/sssaj2013.12.0535.

Widomski, M. K., Sobczuk, H. & Olszta, W. 2010 Sand-filled drainage ditches for erosion control: effects on infiltration efficiency. *Soil Science Society of America Journal* **74** (1), 213–220. doi:10.2136/sssaj2009.0003.

Xie, H. W., Wu, Y. W. & Wang, L. P. 2019 Comparing simulations of green roof hydrological processes by swmm and hydrus-1d. *Water Science & Technology Water Supply* **20** (1), 130–139. doi:10.2166/ws.2019.140.

Young, M. H., Karagunduz, A., Nimůnek, J. & Pennell, K. D. 2002 A modified upward infiltration method for characterizing soil hydraulic properties. *Soil Science Society of America Journal* **66** (1), 57–64. doi:10.2136/sssaj2002.5700.

First received 16 August 2021; accepted in revised form 12 April 2022. Available online 23 April 2022